PeerJ Computer Science

Palmprint recognition based on principal line features

Hongxia Wang and Teng Lv

School of Big Data and Artificial Intelligence, Anhui Xinhua University, Hefei, Anhui, China

ABSTRACT

With the increasing prevalence and diversity of imaging devices, palmprint recognition has emerged as a technology that better meets the demands of the modern era. However, traditional manual methods have limitations in effectively extracting palmprint principal line features. To address this, we introduce a novel data augmentation method. First, the wide line extraction (WLE) filter is utilized to specifically target and extract the prominent principal lines of palmprints by leveraging their direction and width characteristics. Then, a Gabor filter is applied to the WLE-extracted results to purify the features and remove fine lines, as fine lines can introduce noise and redundancy that interfere with the accurate extraction of significant principal line features crucial for palmprint recognition. Evaluating this data augmentation across four common Vision Transformer (ViT) classification models, experimental results show that it improves the recognition rates of all databases to varying degrees, with a remarkable 32.9% increase on the high-resolution XINHUA database. With the successful removal of fine lines by WLE, we propose a new Layer Visual Transformer (LViT) design paradigm. For its input, distinct blocking strategies are adopted, carefully designed to partition the data to capture different levels of spatial and feature information, using larger blocks for global structure and smaller ones for local details. The output results of these different blocking strategies are fused by "sum fusion" and "maximum fusion", and the local and global features are effectively utilized by combining complementary information to improve the recognition performance and get state-of-the-art results on multiple databases. Moreover, LViT requires fewer training iterations due to the synergistic effects of the blocking strategies, optimizing the learning process. Finally, by simulating real-world noise conditions, we comprehensively evaluate LViT and find that, compared with traditional methods, our approach exhibits excellent noise-resistant generalization ability, maintaining stable performance across the PolyU II, IIT Delhi, XINHUA, and NTU-CP-V1 databases.

Subjects Algorithms and Analysis of Algorithms, Artificial Intelligence, Computer Vision, Data Mining and Machine Learning, Security and Privacy

Keywords Data augmentation, Layer visual transformer, Palmprint recognition, Multi-patch, Wide line extraction

Submitted 29 January 2025
Accepted 17 July 2025
Published 18 August 2025

Corresponding author
Hongxia Wang,
wanghongxia@axhu.edu.cn

Academic editor
Paulo Jorge Coelho

Additional Information and Declarations can be found on page 23

DOI **10.7717/peerj-cs.3109**

INTRODUCTION

Palmprint recognition is a critical research topic in the field of biometrics. It involves collecting palmprint images, extracting their features, as well as comparing and matching these features to achieve to achieve identity authentication. Palmprint recognition has important application value in the fields of finance, government, medical care, education

and other domains (*Minaee et al., 2023*). For instance, palmprint recognition can be employed in banks for identity verification, in governments for citizen authentication, in hospitals to enhance patient privacy protection, and in schools to secure student records, among other applications. Compared with other biometric technologies, palmprint has a more stable shape and unique texture information, and offers advantages including easy collection, low cost, and high security. According to whether the palm touches the equipment or not, the palmprint acquisition can be divided into contact and non-contact methods. Compared with non-contact acquisition, contact acquisition helps to ensure the stability of the sensor and the acquisition environment, resulting in better image quality. With the popularization and diversification of imaging equipment, non-contact acquisition can avoid contact between the palm and any object, resulting in low invasiveness, high reliability, and strong social acceptance. At the same time, it makes the palmprint image acquisition more flexible and convenient, and can also provide sufficient palm print information, so it has gradually become the mainstream approach in palmprint recognition systems (*Fei et al., 2019*; *Li et al., 2024*).

As we all know, palmprints are composed of wrinkles and principal lines. The principal lines can be used as an independent feature of the palm. Therefore, there are several reasons to carefully study the method based on the principal lines. Firstly, the method based on the principal lines can be integrated with human behavior. For example, when humans compare two palmprints, they visually compare the principal lines. Secondly, principal lines are generally more stable than wrinkles. Wrinkles are easily concealed by poor lighting conditions, compression artifacts, and noise in real-world environments. Thirdly, the principal line can be used as an important component of multi-feature methods. Finally, due to their simplicity, principal lines can be used for palmprint classification or fast retrieval systems. However, up to now, the method based on the principal line has not been fully studied. The main reason is that complex palmprint images often contain prominent and extensive wrinkles, which makes it challenging to extract the principal lines. Additionally, many researchers believe that it is difficult to achieve high recognition rates only by using the principal line due to the similarity among individuals (*Zhang et al., 2003*). However, there have been no relevant experiments conducted to verify their views.

Obviously, lines are the basic features of palmprints. Therefore, line-based methods also play a significant role in the field of palmprint verification and recognition. Due to slight variations in pose, rotation angle, and illumination intensity during non-contact image acquisition, directly using the extracted principal lines for matching verification often yields unsatisfactory results. The common matching method is to measure the similarity distance between the principal lines of two samples. Because the process of extracting the principal lines is rough, the extracted principal lines are often purified first, but there is still no unified method to effectively deal with all kinds of fine lines, so it is urgent to find a universal matching scheme. Deep learning is a good way to learn target features from a local perspective, which is usually not affected by slight deformations, distortion, translation and other factors. Therefore, the principal line discrimination based on deep learning can meet the needs of the palm print recognition system with non-contact and

union constraints better than traditional methods. As a paradigm shift in the field of computer vision, Vision Transformers (ViTs) use the transformer architecture to achieve first-class performance in image classification tasks, while providing efficiency, flexibility, interpretability and scalability. This article applies ViTs to palmprint principal line matching tasks, and achieves state-of-the-art results in three databases.

This article mainly studies deep learning palmprint recognition algorithm. The main contributions of this research are as follows.

(1) We propose a new filter named wide line extraction (WLE). This innovation is of great significance, because before our work, the existing palmprint line extraction methods failed to fully consider the width and direction characteristics of palmprint lines. WLE filtering can extract more prominent lines from palmprint images. Specifically, WLE is a new technology, which takes into account the characteristics of the palmprint line itself, such as its direction and width. Traditional methods mainly focus on local texture or edge features, and lack the ability to extract lines based on their inherent geometric characteristics. By doing so, WLE not only improves the clarity of palmprint line extraction, but also simplifies the data processing flow, making it a valuable contribution in the field of palmprint recognition.

(2) We propose a novel layered ViT (LViT) architecture. Unlike conventional models, LViT leverages the unique block structures of different palmprint images by fusing multiple block branches. This innovative approach not only boosts recognition accuracy but also cuts down training time, enabling it to achieve state-of-the-art performance in palmprint recognition.

(3) The proposed LViT architecture has good anti-noise generalization capability. We simulated some bad conditions in the actual situations (such as rain, storm and dust), and added salt-and-pepper noise, Gaussian noise and random occlusion to all the dataset. The overall recognition performance of our method clearly outperforms the performance of previous state-of-the-art methods.

(4) We provide a high-resolution palmprint database named XINHUA.

RELATED WORK

Image line features retain important information about the shape of objects in the scene and play an important role in advanced tasks, including matching and recognition (*Davis, Rosenfeld & Agrawala, 1976*). Generally, palmprint recognition uses the palm of a person to identify or verify their identity (*Li et al., 2009*). Palmprint has many important features, such as principal lines, wrinkles, ridges, minutiae and textures. Among these features, the principal line, as one of the most obvious features of palmprints, has always been a focus research topic (*Wu, Wang & Zhang, 2002*). Usually, palmprints contain three principal lines: heart line, head line and life line (*Huang, Jia & Zhang, 2008*). If three smooth and noiseless principal lines can be extracted as feature images, it will lay a good foundation for fast matching and recognition for later. Therefore, extracting the principal lines of palmprint is crucial for palmprint recognition. Up to now, palmprint recognition has studied many algorithms for line detection and matching, including those based on palmprint principal lines and texture lines (some tiny short lines and

ridges), which are mainly divided into traditional methods and deep learning-based methods.

In traditional palmprint line extraction methods, detectors are generally designed manually to extract line features. Early studies mainly focused on basic feature detection and matching. For instance, *Wu, Wang & Zhang (2002)* designed a set of line detectors to assess the smoothness, connectivity, and width of lines, employing the Hausdorff distance for line matching. In the context of low-resolution palmprint recognition, *Wu et al. (2004)* developed a set of directional line detectors, along with a new automatic classification algorithm based on the width and thickness of palmprint principal lines.

As research progressed, some scholars began to focus on extracting principal lines from the characteristics of images. *Liu & Zhang (2005)* obtained the intensity relationship between palmprint lines by minimizing local image regions with similar brightness to each pixel, thus extracting the principal lines of palmprints. *Wu & Zhang (2006)* extracted line features in different directions and represented some fine lines using chain codes. During the matching stage, they performed matching based on the distances between points on the palmprint lines. *Liu, Zhang & You (2007)* adopted an isotropic nonlinear filter as a wide-line detector from the perspective of line width, achieving a relatively robust line extraction effect.

Meanwhile, methods based on transformation and retrieval gradually emerged. *Huang, Jia & Zhang (2008)* utilized the improved finite radon transform (MFRAT) to extract the principal line features of palmprints and employed a "point-to-region" approach for matching, achieving good results. *Jia et al. (2009)* proposed a fast palmprint retrieval scheme based on principal lines, leveraging the position and direction of key points on principal lines to retrieve palmprints, which achieved extremely fast retrieval results while ensuring good accuracy. *Li et al. (2009)* first used MFRAT to extract the preliminary principal lines of palmprints and then obtained the final refined principal lines through post-processing operations such as binarization and morphology.

Subsequent research further deepened the combination of preprocessing and feature optimization. *Li, Liu & Zhang (2010)* first preprocessed the images (such as median filtering, *etc.*), then refined the detected palmprint lines based on diversity and contrast, and used edge tracking to remove thin branches and short lines to obtain the principal lines of palmprints. *Yuan et al. (2011)* designed a dotted-link algorithm using the principal line tracking method, taking into account the specific direction of principal lines and the prior knowledge of valley edges. *Rotinwa-Akinbile, Aibinu & Salami (2011)* treated the principal lines of palmprints as edge detection, using Sobel operators in both horizontal and vertical directions to extract principal lines and applying discrete Fourier transform technology to calculate the distances from endpoint to endpoint for matching.

In addition, innovative methods based on morphology and edge detection continued to emerge. *Kalluri, Prasad & Agarwal (2012)* designed a set of wide principal line extractors, using morphological operators and grouping functions to eliminate noise. During the matching stage, they developed a matching algorithm based on pixel comparison to calculate the similarity between palmprints. *Di, Shi & Xu (2013)* first used Nibrack's

method to roughly segment the principal lines of palmprints, then applied the SUSAN operator to limit the range of principal lines as the localization result, and finally achieved accurate extraction of palmprint principal lines through the intersection of rough-segmentation and localization results. *Biradar (2013)* proposed using canny edge detection to extract principal line features, using Sobel masks to find the edge direction and gradient intensity of each pixel in the preprocessed image, and then tracking the edges. Finally, non-maximum edges were suppressed by identifying parallel edges and eliminating those with weaker gradient strength. *Bruno et al. (2014)* achieved a simple, efficient, and accurate method for extracting palmprint principal lines through image normalization, median filtering, average filtering, gray combined filtering, binarization, and post-processing.

In recent years, research directions have expanded towards multimodality and algorithm innovation. *Iula & Nardiello (2016)* proposed a biometric recognition method based on ultrasound. In the same year, *Ali, Yannawar & Gaikwad (2016)* used local entropy information and local variance for edge detection, exploring the potential of some classical edge operators (such as the Sobel operator, *etc.*) in extracting palmprint principal lines. *Sathish, Baskar & Kumar (2021)* used the Prewitt edge detector, Sobel operator, canny edge detector, Kirsch operator, and multi-scale edge detector to extract the features of palmprint lines.

In terms of algorithm optimization, recent studies have made remarkable progress. *Wang & Mariano (2024)* proposed a local ordinal code (LOC) using three common filters for multi-lines-directional filtering coding to overcome the high computational cost and low accuracy of traditional palmprint local recognition methods, introduced a dimension control factor for linear dimensionality reduction to enable large-scale retrieval, developed FFLOC for feature fusion. *Liao et al. (2024)* proposed boundary line calibration (BLC) and finger valley calibration (FVC) to tackle translational dislocations in the DLSP assisting graph for mobile palmprint recognition. By rotating samples, cropping specific regions, applying Gabor filters, and localizing key features, their method effectively improved recognition accuracy and user comfort. *Wang & Cao (2025)* proposed the bifurcation line direction coding (BLDC) method to overcome challenges in palmprint recognition like image variability and limitations of traditional single-line-feature-based methods. Using an improved Gabor filter for preprocessing and generating feature codes based on main direction subscripts.

Deep learning, as a powerful machine learning technique, is highly regarded in current scientific research and engineering applications. In recent years, with the continuous development and optimization of deep learning models, the applications of deep learning in various fields have become increasingly widespread and profound. Studies in COVID-19 early diagnosis (*Zivkovic et al., 2022*; *Jain et al., 2023*), geological disaster prediction (*Chen & Song, 2023*), financial market forecasting (*Mousapour Mamoudan et al., 2023*), and pedestrian detection (*Jain et al., 2023*) have all demonstrated the outstanding performance of combining deep learning with metaheuristic optimization algorithms in solving complex problems. These studies not only overcome the limitations of traditional algorithms but also provide new ideas and methods for future academic research and

practical applications. The popularity of deep learning is attributed to its enormous potential and continuous exploration in solving complex real-world problems. Some researchers have gradually turned to deep learning to perform palmprint line extraction. *Wang et al. (2013)* proposed a method to quickly extract palmprints using image data field and pulse-coupled neural network (PCNN). *Putra et al. (2021)* and other researchers added edge detection results to convolutional neural network data for training purposes. *Zhao et al. (2022)* proposed synthesizing training data by processing palmlines. These studies verify that deep learning can effectively perform palmprint line extraction. *Parulan, Borcelis & Linsangan (2024)* proposed an innovative dynamic image segmentation-based approach for palm line identification and analysis, using palm line images captured by a device as biometric data, implementing percentage error for statistical treatment. *Jia & Zhou (2024)* proposed UC-HRNet, a high-resolution network for palmprint principal line extraction, aiming to address the challenges in dense prediction tasks of semantic segmentation. Leveraging the parallel feature map preservation of HRNet and the effective feature fusion of UNet's U-shaped structure with skip connections, and using deep supervision for hierarchical feature representation. In recent years, cross-domain palmprint recognition is mostly used in transfer learning, aiming at bringing the knowledge learned in one domain to another domain to realize domain adaptation. *Shao, Zhong & Du (2019)* proposed PalmGAN to address cross-domain palmprint recognition by generating labeled fake images that reduce domain gaps while preserving identity information. *Ruan, Li & Qin (2024)* proposed LSFM, an efficient light style and feature matching method for cross-domain palmprint recognition, addressing the challenges of domain shifts and resource limitations. *Xin et al. (2024)* proposed a self-attention CycleGAN for cross-domain semi-supervised palmprint recognition, addressing challenges in contactless palmprint recognition with different devices and limited labeled data. In the future, with the emergence of more cross-domain methods, such as those based on generative adversarial networks (GANs) and self-attention mechanisms, cross-domain palmprint recognition is expected to significantly enhance accuracy and efficiency in real-world applications. Additionally, strategies that combine small amounts of labeled data with unsupervised learning will further drive the adoption of cross-domain palmprint recognition in practical settings, especially in areas like security authentication and smart access control.

PALMPRINT DATASET

This study utilizes five palmprint datasets: PolyU II (*Bruno et al., 2014*), IIT Delhi (*Kumar & Shekhar, 2011*), XINHUA (*Wang & Mariano, 2024*), NTU-CP-V1 (*Matkowski, Chai & Kong, 2020*), and BJTU-V2 (*Chai, Prasad & Wang, 2019*). This section describes the characteristics, collection methods, and advantages of each dataset. Table 1 summarizes the key detail of the five palmprint datasets.

This work utilized PolyU II palmprint database sourced from http://www4.comp.polyu.edu.hk/~biometrics/, utilized IIT Delhi Touchless Palmprint Database sourced from https://www4.comp.polyu.edu.hk/~csajaykr/IITD/Database_Palm.htm,

Table 1 Introduction to palmprint dataset.

Dataset	Attribute			
	Is it a restricted environment	Number of collectors	Number of categories	Total number of images
PolyU II (2014)	Yes	193	386	7,752
IIT Delhi (2011)	Yes	230	460	2,601
XINHUA (2024)	Yes	50	100	2,000
NTU-CP-V1 (2020)	No	328	655	2,478
BJTU-V2 (2019)	No	148	296	2,663

utilized XINHUA Palmprint Database sourced from https://github.com/HewelXX/Dataset/tree/main/XINHUA, utilized NTU-CP-v1 Palmprint Database sourced from https://github.com/matkowski-voy/Palmprint-Recognition-in-the-Wild, utilized BJTU-V2 Palmprint Database sourced from https://github.com/HewelXX/Dataset/tree/main/BJTU_V2.

PolyU II

The PolyU II dataset is a widely used contact-based 2D palmprint database. The dataset comprises 386 palms from 193 participants, covering both left and right hands. The data collection was conducted in two phases with a two-months interval between, with approximately 10 palmprint images collected per phase in each, resulting in a total of 7,752 images. The PolyU II is renowned for its large sample size and distinct palmprint features, making it widely used in palmprint feature extraction and matching research. Its advantages lie in its abundant samples and well-standardized collection process, while its limitation stems from its sole focus on contact-based collection environments, which results in a lack of diversity in non-contact scenarios.

IIT Delhi

The IIT Delhi dataset is a contact-based palmprint database comprising 2,601 images from 460 palms of 230 participants. For each palm, five to seven images were captured under different hand postures. The dataset includes both raw palmprint images and normalized, cropped images (150 × 150 pixels), which facilitates research and comparison among feature extraction algorithms. The advantage of IIT Delhi dataset lies in its inclusion of diverse hand postures and normalized images, which makes it an ideal data source for comparative analysis of palmprint images under varying conditions.

XINHUA

The XINHUA dataset is a high-resolution palmprint database developed specifically for this study, aiming to provide richer data support for palmprint recognition research. The dataset includes 2,000 palmprint images from 50 participants, comprising 41 males and nine females, all aged 20 to 30. The data collection was conducted in two phases, from January 2022 to April 2022, with each participant providing 10 images of their left hand and 10 images of their right hand during each phase.

The data was collected using an iPhone XR smartphone in an indoor setting, with fixed lighting conditions and a stable shooting distance of approximately 20 centimeters. During the collection process, participants were asked to spread their palms flat, avoid occlusion and excess shadows, and ensure a simple and clean background. The data are stored in high-resolution image format, facilitating the extraction of palmprint feature details. Using a smartphone as the collection device makes the dataset more relevant to real-world applications, improving its practicality and usability. A standardized collection protocol ensures consistency in data quality.

NTU-CP-V1

The NTU-CP-v1 is a contactless palmprint database comprising 2,478 images from 655 palms of 328 participants. The participant pool is predominantly of Asian descent (including Chinese, Indian, and Malay), with a small number of Caucasians and Eurasians. The data collection was conducted in two phases, in everyday indoor environments in Singapore, with no strict posture requirements. The images were captured using Canon EOS 500D and Nikon D70s cameras, ensuring high image quality. The advantage of NTU-CP-v1 lies in its contactless collection, which more closely resembles real-world usage scenarios. Additionally, it covers a diverse range of ethnic backgrounds, providing significant support for cross-ethnic palmprint feature research.

BJTU-V2

The BJTU-V2 dataset comprises 2,663 hand images from 148 volunteers (91 males and 57 females), with ages ranging from 8 to 73 years. The data collection was conducted in two phases, from November 2015 to December 2017, with each participant providing three to five images of their left hand and three to five images of their right hand during each phase. The images were captured using various smartphones (such as iPhone 6, Nexus 6P, Huawei Mate8, *etc.*) in both indoor and outdoor settings.

DATA AUGMENTATION OPERATION

Data augmentation is a technology for artificially expanding the training dataset by generating more equivalent data from limited data. It is an effective means to overcome the shortage of training data, and it is widely used in various fields of deep learning. In this article, a WLE filter is proposed to perform preliminary line extraction on the original image, and the specific filter template is shown in Fig. 1. Due to the complexity of the legend, only one direction of the filter template is listed in Fig. 1A (template size is 13×13, in the actual extraction process, the template size is set to 35×35). The templates in Figs. 1B and 1C present simplified diagrams, in which Fig. 1B illustrates the left-hand template and Fig. 1C illustrates the right-hand template. It should be noted that the red curve in Fig. 1A has the same functional representation as the red curves in Figs. 1B and 1C, both of which denote the template direction.

The choice of left-hand and right-hand templates is based on both empirical observations and experimental validation. From an empirical perspective, the left-hand

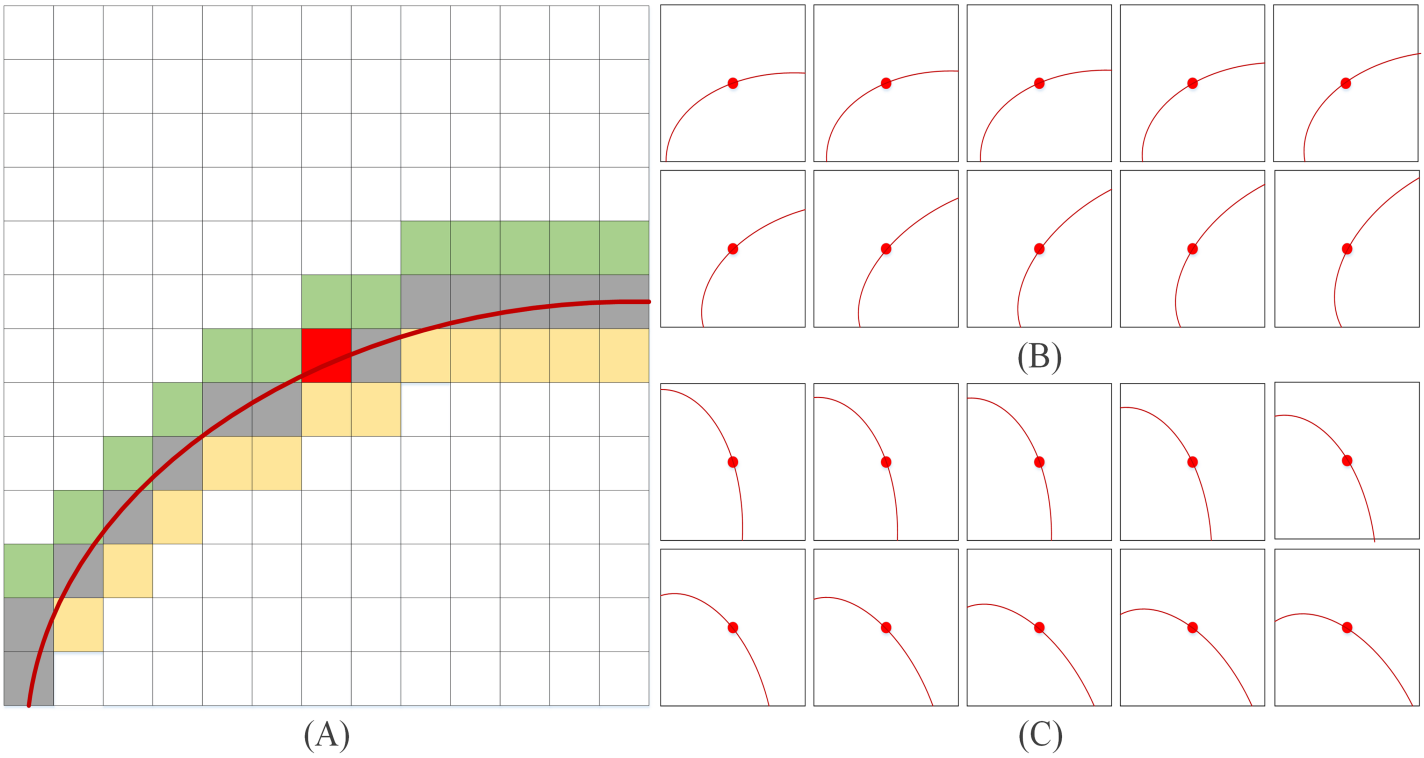

Figure 1 WLE filter. (A) Only one direction of the filter template (B) left-hand template (C) right-hand template.
Full-size DOI: 10.7717/peerj-cs.3109/fig-1

and right-hand directions correspond to the natural orientations of most palmprint lines, ensuring that the templates align well with the dominant features. Experimentally, multiple template configurations were assessed he left-hand and right-hand templates exhibited superior performance in significantly improving line extraction accuracy and robustness. Furthermore, as illustrated in Fig. 1A, the width of template line direction is set to three pixels, as the principal palmprint lines typically have a width ranging from two to five pixels (*Jia, Huang & Zhang, 2008*).

When performing convolution filtering, WLE sums all pixel values within a region of three-pixel width. The specific equation is given by Eq. (1)

$$I_{WLE} = I * WLE \tag{1}$$

where WLE is defined as follows:

Given $Z_p = \{0, 1, \ldots, p-1\}$, where p is a positive number representing the size of the grid, on a finite grid $Z^2{}_p$, the real-value function of WLE is given by Eq. (2), where k represents the width of the line, L_k denotes the set of points that make up a line on the lattice $Z^2{}_p$, $f[x, y]$ is the gray value on the image I, ρ is a limiting parameter to prevent the sum of gray values from exceeding 255, and ρ ranges from 0 to 1. It is worth noting that before using WLE to perform convolution filtering, it is necessary to use mean reduction to preprocess the image, that is, $I = I' - mean(I')$.

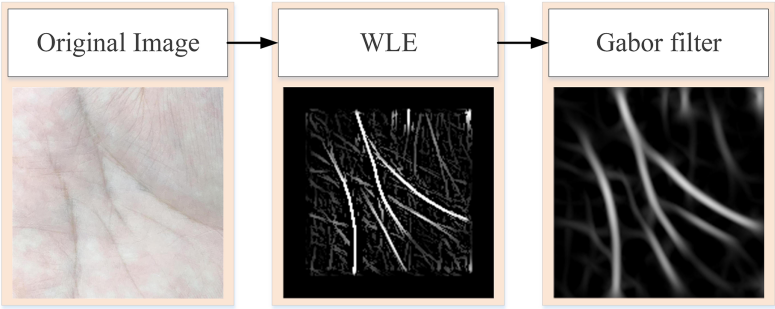

Figure 2 **Process of extracting pure palmprint principal line.**
Full-size DOI: 10.7717/peerj-cs.3109/fig-2

$$WLE(k) = \rho \sum_{k=1}^{3} \sum_{(i,j)\in L_k} f[i,j]. \tag{2}$$

WLE only preliminarily screens the more obvious lines in the palm, such as some fine cross lines. To obtain the more obvious principal lines of the palmprint, further data preprocessing operations are needed. Figure 2 is the flowchart of obtaining the principal line of palmprint. First, the original palmprint image is processed by WLE filter, and then the filtered image is convolved by Gabor filter to remove any fine lines that remain after WLE processing.

LAYERED VISUAL TRANSFORMER PARADIGM

Previously published material must be accompanied by written permission from the author and publisher. ViT's idea is to divide the image into blocks and send these blocks to the encoder, which inevitably leads to the question of whether all images are suitable for the same blocking strategy? The process of the model learning different things is both difficult and easy. Simple images are easy to identify and do not require dividing the image into multiple patches for training. However, dividing the image into multiple patches can lead to the shortcomings of long training time and insufficient precision. Therefore, this article introduces LViT, a Layered ViT model paradigm. The core idea is straightforward: the input image is divided into different numbers of patches for separate training, and the linear results of each patch number are summed and fused to output. Figure 3 illustrates the architecture of the LViT paradigm (here using only two blocking methods as examples). LViT extends the transformer architecture to enable multiple classification token head outputs. To distinguish the number of blocks between multiple modalities, we expanded the original Transformer architecture to include one-dimensional multi-patch embedding, which marks each blocking method and enhances network's generalization ability.

Here, ViT (*Dosovitskiy et al., 2021*) is taken as an example and its formula is followed, which is supplemented and explained in detail. In Eq. (3), Z represents the output set of all different blocks, where z_i represents the output of each block scheme (Eq. (4)). Here, M

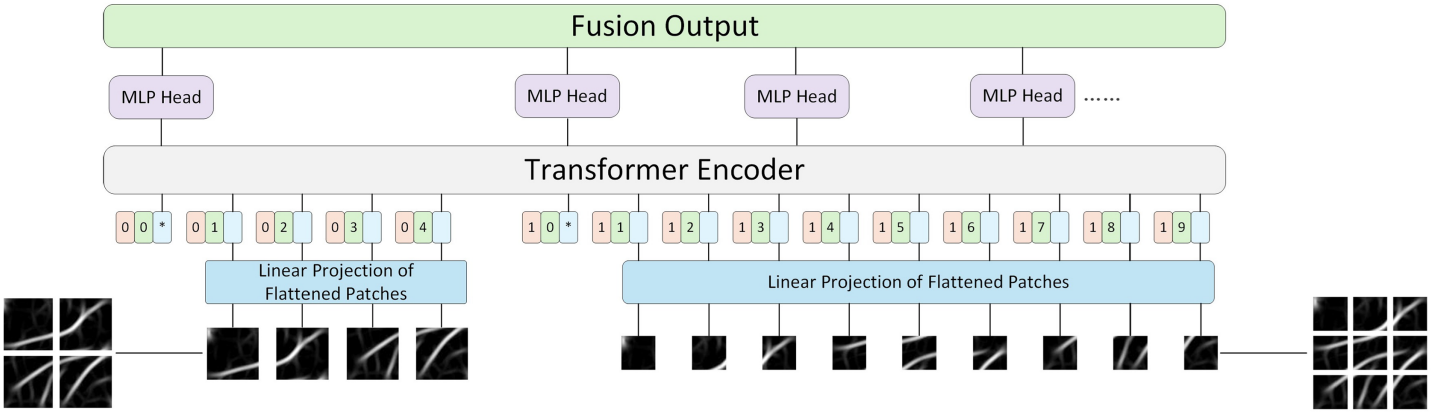

Figure 3 **LViT papadigm.** Full-size DOI: 10.7717/peerj-cs.3109/fig-3

represents the number of types of block schemes, N represents the number of blocks in each block scheme, $x_{multi-patch}$ and x_{class} are two learnable embeddings, representing the block-level and category-level embeddings, respectively, and x_p represents the sequence of flattened 2D patches, $\mathbb{R}$ represents real numbers, P^2 represents the resolution of each image patch, C represents the number of image channels, and D represents the dimension of Transformer mapping layer.

$$Z = [z_0;\ z_1;\ z_2;\ \ldots;\ z_M]. \tag{3}$$

$$z_i = \left[x_{multi-patch};\ x_{class};\ x_p^1 E;\ x_p^2 E;\ldots;\ x_p^N E;\right] + E_{pos},$$
$$E \in \mathbb{R}^{(P^2\cdot C)\times D},\ E_{pos} \in \mathbb{R}^{(N+1)\times D},\ i = 1,\ldots,M. \tag{4}$$

Next, in order to obtain the final classification result of each block scheme, this article did not directly use the concatenated result in Eq. (3) as the input in the Encoder part, but sent each block scheme into the Encoder as a different input for separate training. This approach aligns with the original encoder parameter settings of ViT, thereby enhancing training efficiency for future transfer learning applications. Equations (5), (6) and (7) are the multi-headed self-attention (MSA), multilayer perceptron (MLP) and LayerNorm (LN) components of the Encoder, respectively. The superscript 1 in z_L^1 in Eq. (7) denotes the dimension index of the class token. In this algorithm, the class token is placed in the first dimension, while multi-patch embedding is in the 0th dimension, which is different from ViT where the class token is in the 0th dimension. L denotes the maximum number of layers in the Encoder.

$$z_l' = MSA(LN(z_{l-1})) + z_{l-1}, \quad l = 1,\cdots,L. \tag{5}$$

$$z_l = MLP\left(LN\left(z_l'\right)\right) + z_l' \quad l = 1,\cdots,L. \tag{6}$$

$$y = LN\left(z_L^1\right). \tag{7}$$

After obtaining each block scheme, this article fuses the results of each scheme to make the final prediction. This approach is referred to as LViT. Specifically, in the corresponding fusion strategy, two fusion methods, namely “sum fusion” and “maximum fusion”, are

adopted to fuse the matching value layer. Equation (8) represents the "summation fusion" method, where N is the number of block types, and S denotes the output score of each block. Equation (9) represents the for "maximum fusion" method.

$$LViT_{Sum} = Sum(S_{block1}, S_{block2}, \ldots, S_{blockN}) = \frac{1}{N} * (S_{block1} + S_{block2} + \ldots + S_{blockN}). \quad (8)$$

$$LViT_{\mathrm{Max}} = Max(S_{block1}, S_{block2}, \ldots, S_{blockN}). \quad (9)$$

DISCUSSION AND ANALYSIS OF EXPERIMENTAL RESULTS

In this section, the Transformer architectures used are the existing backbone networks, namely ViT, Conformer (*Peng et al., 2021*), PVT-V2 (*Wang et al., 2022*) and ConvMixer (*Trockman & Kolter, 2022*). ViT is the first successful attempt to introduce the Transformer into the vision field, setting a precedent for vision Transformers. ViT converts image data into sequence data and feeds it into the standard Transformer encoder to achieve higher recognition accuracy. Conformer is based on the feature coupling unit (FCU), which fuses local features and global representations under different resolutions in an interactive fashion. Conformer adopts a concurrent structure to maximize the retention of local features and global representations. PVT-V1 (*Wang et al., 2021*) is the first pyramid-structured Transformer model, which proposes a hierarchical Transformer with four stages, demonstrating that a pure Transformer backbone can be as universal as the CNN backbone. PVT-V2, on the other hand, introduces overlapping patch embedding, convolutional feed-forward, and linear spatial reduction attention to improve the recognition accuracy and reduce the computational complexity.

In verify the effectiveness of the proposed method this chapter, this section conducts experimental tests from the following three aspects. (a) Baseline experiments, referring to the training results of the original dataset using various backbone networks; (b) Comparative experiments using WLE data augmentation; (c) Experimental results of LViT paradigm.

In this study, the training strategies and parameter settings for deep models were based on the approach described by (*Zivkovic et al., 2022*), whereas the experimental settings for traditional methods followed those of (*Dosovitskiy et al., 2021*). For deep model training, the training and testing sets were strictly divided according to the collection phases, using data from the first phase as the training set and data from the second phase as the testing set. Since the IIT Delhi dataset has only one collection phase, the first collected sample from each class was used as the training set, and the remaining samples were used as the testing set. Regarding the image size, images from different databases varied significantly. The original palmprint image size ranges from 128 × 128 pixels to 2,000 × 2,000 pixels. To ensure compatibility with our models and maintain computational efficiency, we resized all images in this dataset to a fixed size of 224 × 224 pixels using the bilinear interpolation method. A detailed summary of these division strategies for all databases is presented in Table 2 for easy reference. For deep learning methods, the batch size for training was set to 4, the learning rate to 5×10^{-5}, the optimizer to AdamW

Table 2 The division strategies for all databases.

Dataset	Train number of training sets	Test number of training sets	Original palmprint image size	Input the palmprint image size of the model
PolyU II	3,889	3,863	128 × 128	224 × 224
IIT Delhi	459	2,237	150 × 150	224 × 224
XINHUA	1,000	1,000	2,000 × 2,000	224 × 224
NTU-CP-V1	1,304	1,086	About 500 × 500 resolution	224 × 224
BJTU-V2	1,341	1,322	About 1,000 × 1,000 resolution	224 × 224

Table 3 The main evaluation index of palmprint recognition system.

Evaluation index	Abbreviation	Description
False rejection rate	FRR	The proportion of genuine being incorrectly rejected by the classifier.
False acceptance rate	FAR	The proportion of impostors mistakenly judged as accepted by the classifier.
Genuine acceptance rate	GAR	The concept of GAR is opposite to FRR, with a value of 1-FRR.
Receiver operating characteristic	ROC	The receiver operating characteristic intuitively reflects the balance relationship between GAR and FAR at different thresholds of the recognition algorithm, where the horizontal axis is FAR and the vertical axis is GAR.
Equal error rate	EER	The value of the ROC curve when FRR and FAR are equal.
Accuracy recognition rate	ARR	The ratio of correctly classified samples to total samples

Table 4 Baseline experimental results of each dataset in the restricted environment.

Methods	Patch size	PolyU II		IIT Delhi		XINHUA	
		ARR	EER	ARR	EER	ARR	EER
ViT-B	16	87.78	7.1427	76.64	14.3725	38.90	45.3584
	32	80.09	10.2715	70.15	20.4975	35.80	49.2105
Conformer-B	16	91.98	6.1325	81.19	9.3667	46.20	37.3344
	32	86.35	7.4487	74.22	16.3562	38.60	46.7724
PVT-V2-B5	4	95.91	3.7245	91.78	5.9733	71.50	19.2238
	8	95.86	3.7326	91.36	6.0445	73.00	18.1582
	16	95.81	3.8046	89.96	6.8328	71.50	19.2674
	32	96.33	3.3026	90.33	6.7544	77.30	13.9044
ConvMixer	7	99.82	0.7526	92.89	5.7742	69.60	20.8743
	14	99.85	0.6344	89.47	6.9804	63.80	23.5576

(*Loshchilov & Hutter, 2018*), and data augmentation was implemented using RandAugment (*Cubuk et al., 2020*).

Generally speaking, the system performance evaluation criteria of palmprint recognition algorithm are shown in Table 3. Accuracy recognition rate (ARR), equal error rate (EER), genuine acceptance rate (GAR), false acceptance rate (FAR), receiver operating

Table 5 Baseline experimental results of each dataset in the unrestricted environment.

Methods	Patch size	NTU-CP-V1		BJTU-V2	
		ARR	EER	ARR	EER
ViT-B	16	72.99	18.2326	63.90	23.4826
	32	70.70	20.3879	60.05	24.5527
Conformer-B	16	78.39	12.0726	75.13	15.5475
	32	72.44	18.4275	70.25	20.4431
PVT-V2-B5	4	83.24	9.3327	86.18	8.1022
	8	83.79	9.1872	84.34	9.1786
	16	85.44	8.3976	85.51	8.4725
	32	84.71	9.0547	85.76	8.3720
ConvMixer	7	84.89	9.0128	89.03	6.6547
	14	84.98	8.9744	87.35	7.1438

Table 6 Data augmentation experiment results of each dataset in the restricted environment.

Methods	Patch size	PolyU II		IIT Delhi		XINHUA	
		ARR	EER	ARR	EER	ARR	EER
ViT-B	16	96.32	3.3524	84.74	9.0326	69.00	21.0745
	32	92.51	5.8236	76.84	14.3375	68.70	21.2427
Conformer-B	16	92.07	5.9045	85.07	8.5022	71.20	19.5585
	32	87.23	7.2032	78.57	12.0163	63.80	23.6042
PVT-V2-B5	4	96.01	3.6355	92.33	5.7459	78.10	12.8741
	8	96.06	3.6218	94.20	4.5722	76.90	15.3670
	16	96.37	3.2883	92.51	5.7120	79.40	11.4032
	32	96.96	3.2047	93.64	5.0773	76.90	15.3528
ConvMixer	7	99.87	0.5833	93.42	5.1844	79.60	11.4427
	14	99.87	0.6028	89.87	6.5035	77.30	13.8725

characteristic (ROC) will be used as experimental evaluation indexes in the following experiments.

WLE data augmentation experiment

This section evaluates the experiments with and without WLE data augmentation on five datasets, including three palmprint datasets in restricted environment and two datasets in unrestricted environment respectively. The selected evaluation models included ViT, Conformer, PVT-V2 and ConvMixer. But not limited to these evaluation models, any ViTs model can implement the algorithmic paradigms in this chapter. It should be added that in the current well-established deep learning methods, employing basic data augmentation techniques, such as rotation and cropping, has become a necessary operation. This subsection aims exclusively to demonstrate the effectiveness of the WLE data augmentation method and does not involve comparisons with other non-deep learning augmentation methods (*Cubuk et al., 2020*). Table 4 presents the baseline experiments of

Table 7 Data augmentation experiment results of each dataset in the unrestricted environment.

Methods	Patch size	NTU-CP-V1		BJTU-V2	
		ARR	EER	ARR	EER
ViT-B	16	75.02	16.9456	80.90	10.0302
	32	74.90	17.0188	76.48	15.6884
Conformer-B	16	79.44	11.3356	79.73	11.2562
	32	74.26	17.2163	72.18	18.8629
PVT-V2-B5	4	85.99	8.1320	86.52	8.0421
	8	84.61	9.1128	85.76	8.3546
	16	85.53	8.3853	86.60	8.0225
	32	85.43	8.4015	86.01	8.1125
ConvMixer	7	85.35	8.4726	89.11	6.6325
	14	85.26	8.5877	87.69	7.0844

Table 8 LViT experiment results without WLE data augmentation.

Methods	mode	PolyU II		IIT Delhi		XINHUA		NTU-CP-V1		BJTU-V2	
		ARR	EER	ARR	EER	ARR	EER	ARR	EER	ARR	EER
L-ViT	S	90.44	5.9034	80.35	11.4452	53.90	33.1982	74.06	17.8621	72.30	16.8567
	M	91.02	5.7214	80.88	11.0321	56.20	31.2283	74.22	17.5523	73.20	15.2083
L-Conformer	S	92.00	6.0912	83.45	7.9034	58.90	28.3376	78.93	11.8214	77.29	13.2904
	M	92.02	6.0004	83.92	7.1238	59.40	27.3592	79.11	11.6218	78.44	12.8703
L-PVT-V2	S	96.48	3.2896	92.34	5.7213	78.34	12.9886	85.51	8.3614	86.22	8.0823
	M	96.56	3.2455	93.06	5.0662	79.02	11.9232	85.78	8.2514	86.28	8.0546
L-ConvMixer	S	99.85	0.6134	92.95	5.6713	74.50	15.3893	85.12	8.5893	89.08	6.6507
	M	99.87	0.6016	93.11	5.5523	76.20	14.3328	85.33	8.5012	89.11	6.6425

each dataset (PolyU II, IIT Delhi and XINHUA) in the restricted environment, while Table 5 presents the baseline experiments of each dataset (NTU-CP-V1 and BJTU-V2) in the unrestricted environment.

Next, the palmprint images after WLE data augmentation were evaluated to verify the effectiveness of WLE data augmentation. Table 6 presents the experimental results after data augmentation for the datasets PolyU II, IIT Delhi and XINHUA in the restricted environment, while Table 7 presents the experimental results after data Augmentation for the datasets NTU-CP-V1 and BJTU-V2 in the unrestricted environment. The experimental results show that the ViT model with WLE data augmentation exhibits stronger generalization ability. The recognition rate and EER have been further improved.

LViT experiment

This section evaluates the LViT paradigm. In this article, the backbone network name is renamed by adding a prefix identifier. In the experimental results, S denotes "summation fusion" and M denotes "maximum fusion". In this section, two types of LViT ablation

Table 9 LViT experiment results with WLE data augmentation.

Methods	mode	PolyU II		IIT Delhi		XINHUA		NTU-CP-V1		BJTU-V2	
		ARR	EER	ARR	EER	ARR	EER	ARR	EER	ARR	EER
L-ViT	S	96.68	3.2714	85.03	9.0211	71.20	19.5445	78.45	12.6875	81.30	9.9468
	M	96.96	3.1825	86.14	8.2875	71.60	19.1528	78.76	12.5721	81.45	9.8723
L-Conformer	S	92.44	5.7546	86.54	8.1323	73.30	18.5465	79.88	11.0238	80.65	10.1872
	M	93.17	5.4635	86.93	8.0144	73.30	18.4432	80.15	10.8652	81.20	9.9833
L-PVT-V2	S	97.15	3.0421	94.47	4.1732	78.60	12.2874	86.98	7.8833	87.38	7.3625
	M	97.44	2.9328	94.98	3.9828	79.60	11.3678	87.44	7.4902	87.60	7.1256
L-ConvMixer	S	99.93	0.5624	93.47	5.1221	79.80	11.4279	89.35	6.4805	89.23	6.5546
	M	99.93	0.5525	93.65	5.0136	80.10	10.7454	89.78	6.1736	89.76	6.2045

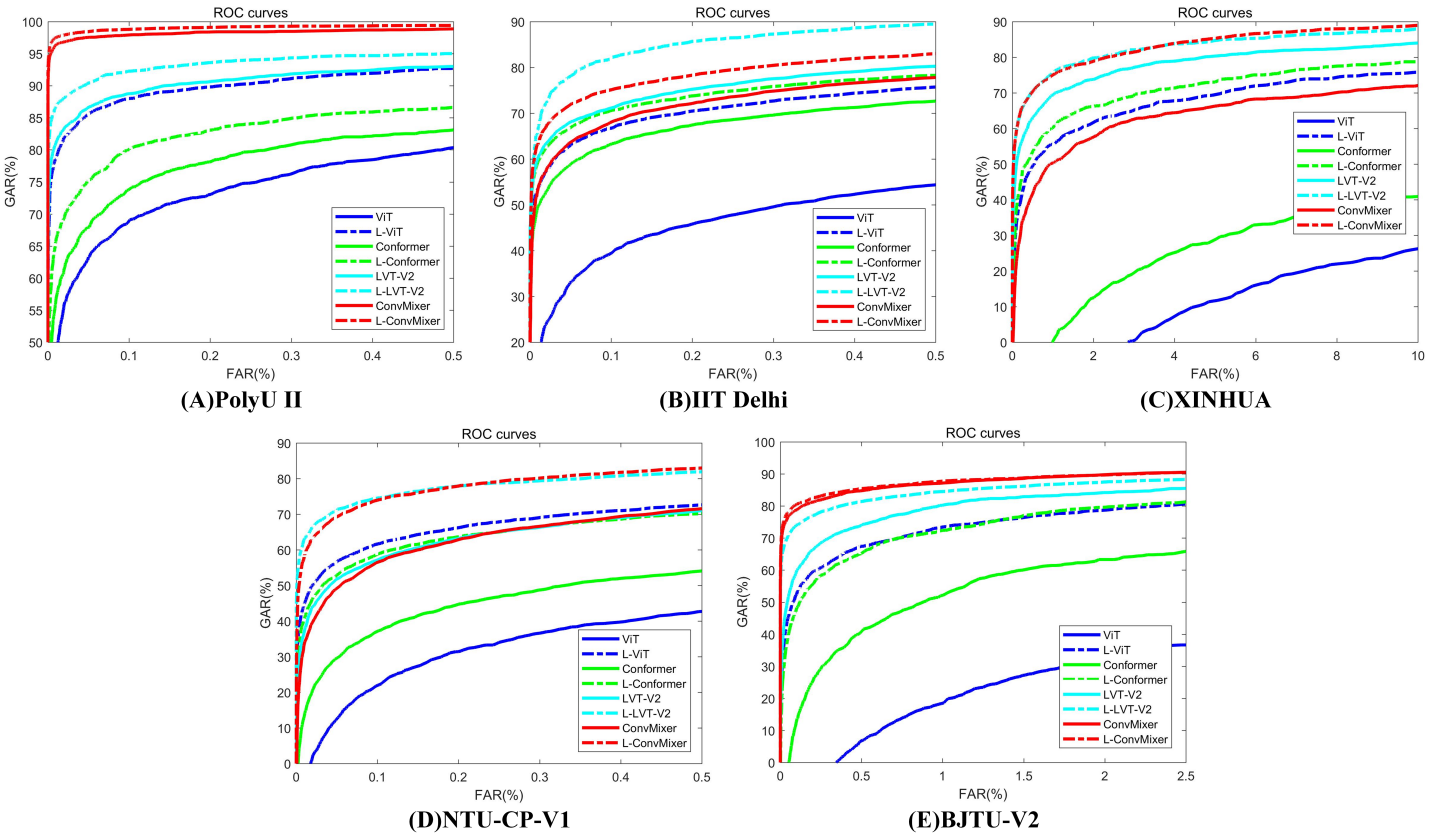

Figure 4 **ROC characteristic curve after WLE augmentation operation.** (A) PolyU II (B) IIT Delhi (C) XINHUA (D) NTU-CP-V1 and (E) BJTU-V2.
Full-size DOI: 10.7717/peerj-cs.3109/fig-4

experiments were conducted, one without WLE data augmentation and the other with WLE data augmentation.

Table 8 presents the experimental results for LViT without WLE data augmentation. It can be seen from Tables 7 and 8 that the augmentation amplitude of WLE is better than that of LViT, that is, the influence of WLE on the model is better than the definition of the

Table 10 Comparative experimental results.

Methods	PolyU II		IIT Delhi		XINHUA		NTU-CP-V1		BJTU-V2	
	ARR	EER	ARR	EER	ARR	EER	ARR	EER	ARR	EER
CompC (*Zhang et al., 2003*)	100	0.0513	89.78	5.4762	79.20	10.6030	89.47	6.7741	87.77	6.6823
OrdinalC (*Sun et al., 2005*)	100	0.0497	88.42	6.2285	73.10	12.0343	87.55	7.5996	88.61	5.4721
RLOC (*Jia, Huang & Zhang, 2008*)	100	0.0521	87.69	6.3400	67.50	15.1470	86.81	7.7674	87.52	6.0517
LLDP (*Luo et al., 2016*)	100	0.0517	91.67	4.3437	76.70	11.2780	88.74	7.7645	91.88	5.3637
EEPNet (*Jia et al., 2022*)	99.67	0.5907	87.65	7.9846	68.40	16.1294	85.07	7.9846	82.75	9.7481
CCNet (*Yang et al., 2023a*)	99.97	0.1554	31.40	40.7147	78.30	14.7012	N/A	N/A	91.04	5.9900
CO3Net (*Yang et al., 2023b*)	99.74	0.2814	64.72	24.3310	72.80	15.1947	70.97	15.5140	87.52	7.7089
L-ViT (Proposed)	96.96	3.1825	86.14	8.2875	71.60	19.1528	78.76	12.5721	81.45	9.8723
L-Conformer (Proposed)	93.17	5.4635	86.93	8.0144	73.30	18.4432	80.15	10.8652	81.20	9.9833
L-PVT-V2 (Proposed)	97.44	2.9328	94.98	3.9828	79.60	11.3678	87.44	7.4902	87.60	7.1256
L-ConvMixer (Proposed)	99.93	0.5525	93.65	5.0136	80.10	10.7454	89.78	6.1736	89.76	6.2045

framework. Table 9 presents the experimental results of LViT with WLE data augmentation. The effectiveness of WLE is further demonstrated in Tables 8 and 9, where the accuracy of ViT and Conformer shows significant improvement. Among them, the M fusion method achieves higher accurate than the S fusion method, because the fusion score takes the maximum score and often can obtain the best selection parameters. The ROC characteristic curve after WLE augmentation operation is illustrated in Fig. 4.

Contrast experiment

In this section, we compare four traditional methods including CompC (*Zhang et al., 2003*), OrdinalC (*Sun et al., 2005*), RLOC (*Jia, Huang & Zhang, 2008*) and LLDP (*Luo et al., 2016*) and three methods based on deep learning including EEPNet (*Jia et al., 2022*), CCNet (*Yang et al., 2023a*) and CO3Net (*Yang et al., 2023b*) to demonstrate the feasibility and effectiveness of LViT. For the sake of fairness, WLE data augmentation operation is used in the comparative experiments of the three deep models, and no other gain operation is performed on the data and models.

Table 10 presents the results of comparative experiments. Due to the manual design of feature extractor, traditional manual methods can often achieve good results in some specific situations, such as PolyU II and NTU-CP-V1. Specifically, LLDP achieved the best performance on BJTU-V2 dataset. However, this does not mean that models based on the LViT paradigm are slightly worse on some specific datasets. This article aims to explain the beneficial effect of the LViT paradigm, but does not dig deep into the benefits brought by model architecture. In addition, it can be seen that the three palmprint recognition methods based on deep learning usually have poor performance. This is because the palmprint dataset is a small sample data, and it is often difficult to identify key features for the model trained from scratch. It is worth noting that CCNet achieves good recognition performance on PolyU II and BJTU-V2 datasets. The images in the NTU-CP-V1 dataset have relatively low resolution, and the sample size for each class is limited. These factors

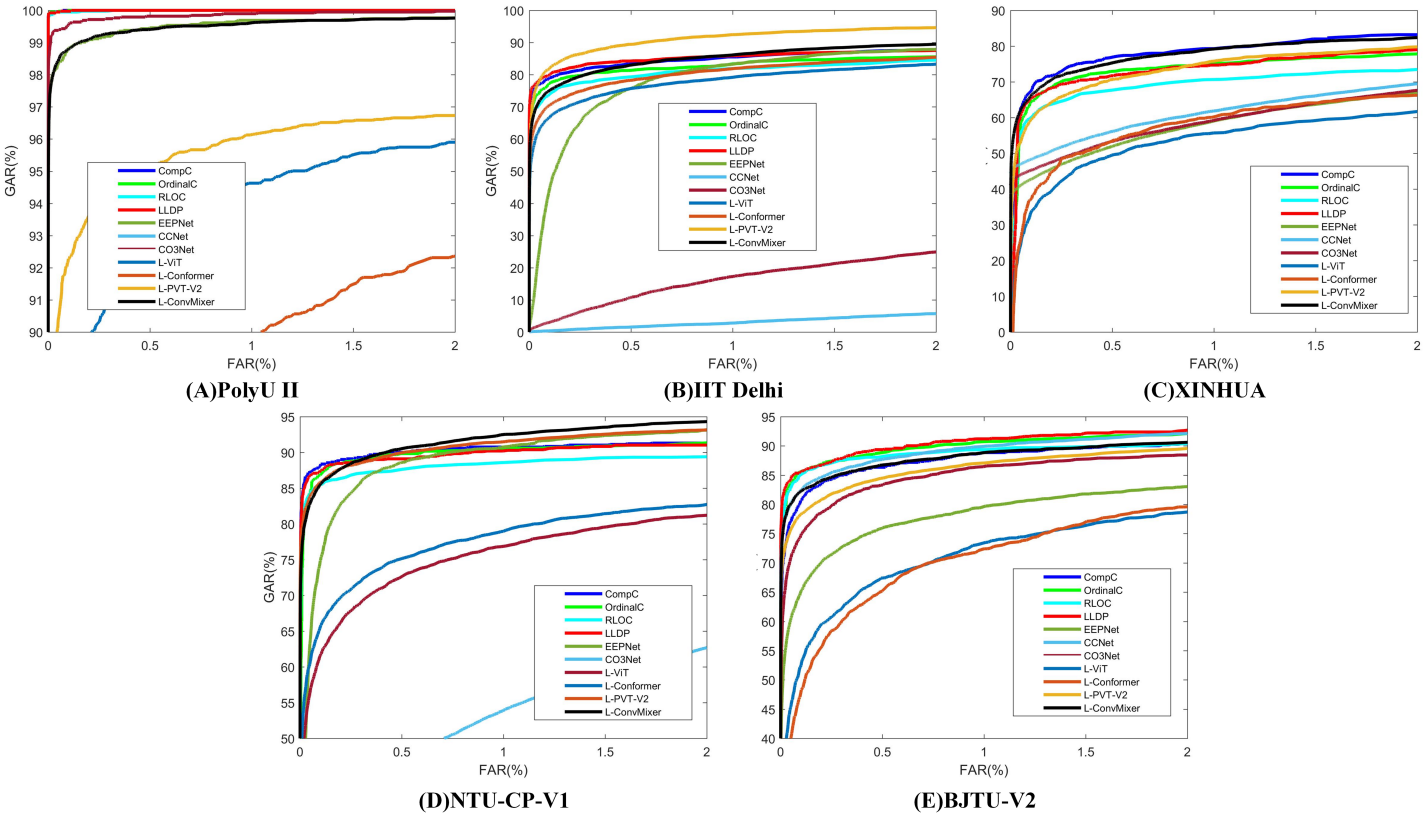

Figure 5 The corresponding ROC characteristic curve of a comparative experiment. (A) PolyU II (B) IIT Delhi (C) XINHUA (D) NTU-CP-V1 and (E) BJTU-V2.
Full-size DOI: 10.7717/peerj-cs.3109/fig-5

cause CCNet's receptive field to fail to effectively capture key features, which in turn affects its training convergence. A ROC characteristic curve of a comparative experiment is illustrated in Fig. 5.

Anti-noise experiment

In real life, there are often worse situations, such as rain, storm, dust, and so on. In these extreme cases, deep learning methods can often exhibit a certain anti-noise capability. However, traditional manual palmprint recognition methods are affected by environmental and terrain factors, leading to reduced recognition. This section simulates several special scenarios and adds noise to palmprint data to verify the effectiveness and generalization ability of the LViT model.

There are three types of preprocessing on palmprint data: salt-and-pepper noise, Gaussian noise and random occlusion. Figure 6 illustrates the example after adding noise, where Fig. 6A illustrates the original image, and Figs. 6B, 6C and 6D illustrate the processing results of salt-and-pepper noise, Gaussian noise, and random occlusion. Table 11 presents the experimental results after noise processing, respectively. The corresponding ROC curve of the anti-noise datasets is illustrated in Fig. 7.

From the above experimental results, we can draw the following conclusions.

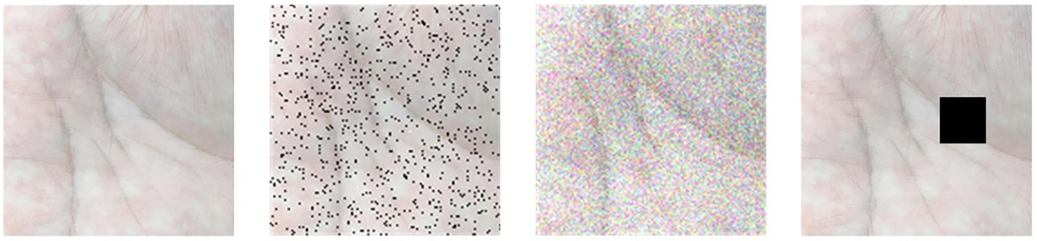

(A) (B) (C) (D)

Figure 6 Add noise processing. (A) Original image (B) salt-and-pepper noise (C) Gaussian noise and (D) random occlusion. Full-size DOI: 10.7717/peerj-cs.3109/fig-6

Table 11 Experimental results of noise.

Methods	PolyU II		IIT Delhi		XINHUA		NTU-CP-V1		BJTU-V2	
	ARR	EER	ARR	EER	ARR	EER	ARR	EER	ARR	EER
CompC (*Zhang et al., 2003*)	91.66	2.5626	84.14	6.7584	75.80	12.6367	85.81	7.6930	56.86	28.2909
OrdinalC (*Sun et al., 2005*)	91.34	2.1021	82.53	8.0058	72.13	12.6926	84.91	8.2385	56.49	19.2576
RLOC (*Jia, Huang & Zhang, 2008*)	93.70	2.1130	78.91	9.4112	69.13	15.0854	83.60	9.3808	51.85	32.6343
LLDP (*Luo et al., 2016*)	84.59	7.2858	81.52	11.3362	71.40	12.4132	80.44	10.1568	58.22	26.5823
EEPNet (*Jia et al., 2022*)	97.44	1.4782	81.47	8.8326	60.47	17.3678	82.33	9.5523	66.92	15.5428
CCNet (*Yang et al., 2023a*)	99.44	0.9725	N/A	N/A	75.97	12.1136	72.80	11.4782	N/A	N/A
CO3Net (*Yang et al., 2023b*)	97.87	1.4033	58.37	18.3925	74.87	12.3217	62.00	16.9084	50.71	33.2165
L-ViT (Proposed)	93.27	2.1896	76.57	12.4426	68.87	15.9838	78.24	11.0236	57.25	25.3416
L-Conformer (Proposed)	91.31	2.6325	80.65	10.3527	73.36	12.6527	85.91	7.5893	46.67	35.7724
L-PVT-V2 (Proposed)	95.99	1.8274	86.15	6.2902	75.80	12.0445	87.53	6.7238	65.83	19.2863
L-ConvMixer (Proposed)	99.53	0.8722	90.58	5.2568	77.40	11.3823	86.00	7.5560	67.39	17.3348

(1) The results of L-ViT are outperform than traditional manual methods in most cases, because ViT benefits from data augmentation, which increases the anti-noise and generalization ability. However, traditional methods are greatly influenced by the environment and are usually suitable for discrimination in a standardized indoor environment;

(2) No traditional method can achieve the best results. Similarly, no L-ViT result is the best in all datasets. This also reflects that the influence of data on the model is uncontrollable. However L-ViT can still mitigate this influence;

(3) The fact that CCNet can be retrained on the NTU-CP-V1 dataset indicates that the data volume determines the model's generalization ability, which aligns with the results in Table 10. Additionally, the IIT Delhi dataset becomes untrainable on the CCNet model when the data volume is increased, possibly due to the extremely limited number of training samples (only one sample);

(4) Traditional manual methods often demonstrate inferior anti-noise performance compared to deep learning-based approaches, because traditional methods rely on

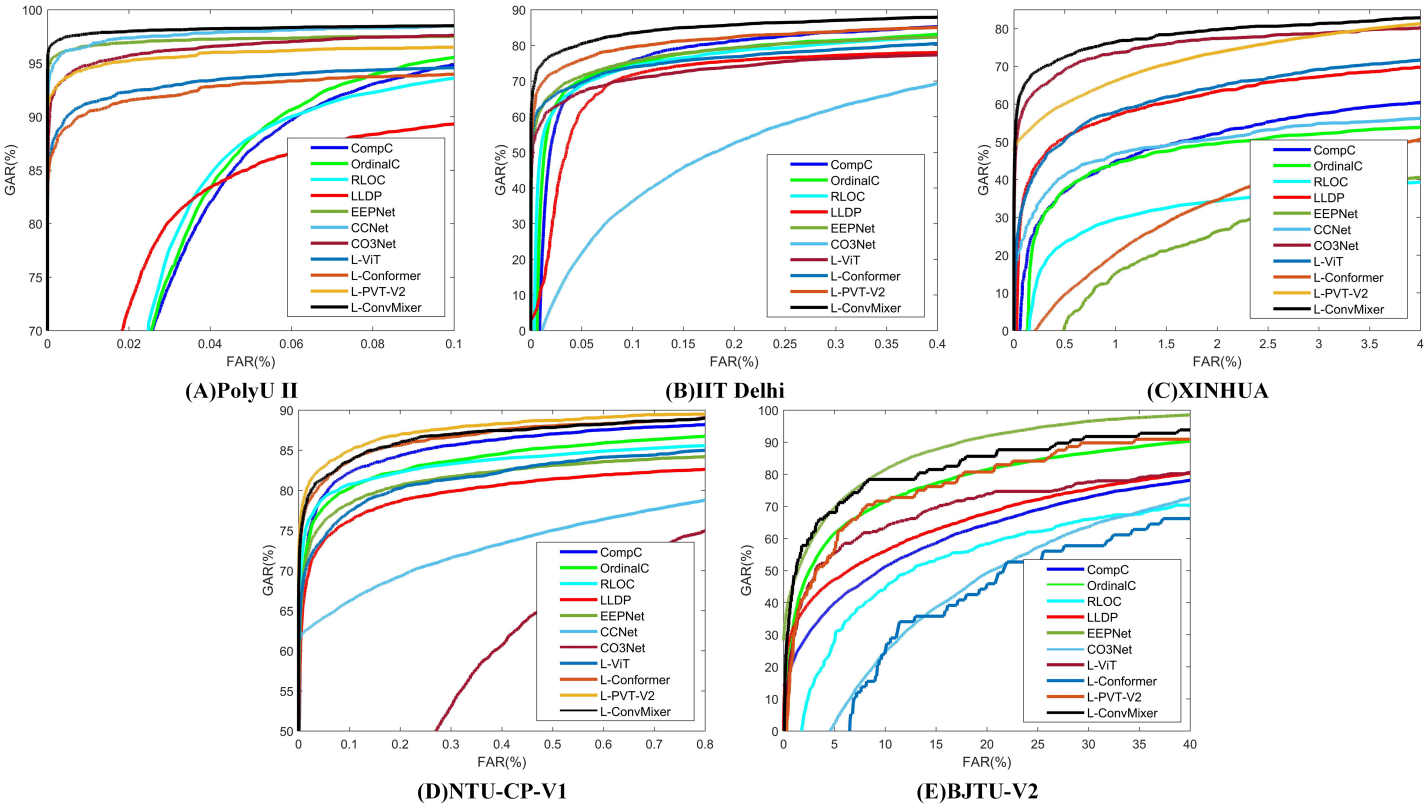

Figure 7 The corresponding ROC curve of the anti-noise datasets. (A) PolyU II (B) IIT Delhi (C) XINHUA (D) NTU-CP-V1 and (E) BJTU-V2.
Full-size DOI: 10.7717/peerj-cs.3109/fig-7

manually designed descriptors, and the feature distribution of the original image changes in an uncertain noise environment;

(5) The experimental results of L-ConvMixer are generally superior compared to other methods, particularly on PolyU II and IIT Delhi datasets.

Discussion and analysis

According to the previous experimental results, the feasibility of the LViT paradigm has been verified, and WLE data augmentation has played a significant role as well. This section focuses on the training time. Since LViT inputs many different patches into the model, it inevitably increases the overall Flops and MAdd of the model. But at the same time, it brings a shorter training time, that is, the number of training iterations is significantly reduced, and the convergence speed of the model is further improved. Figure 8 illustrates the loss function trajectory (with WLE) of each LViT method on the PolyU II dataset. It can be seen that LViT achieves faster convergence with fewer iterations, and its loss function is relatively smooth.

For real-time applications, computational complexity is an important factor to determine the processing speed. In the process of large-scale manual authentication, traditional methods often need to extract features online and match them after processing. Because LViT is based on a deep learning model, real-time matching can be achieved as

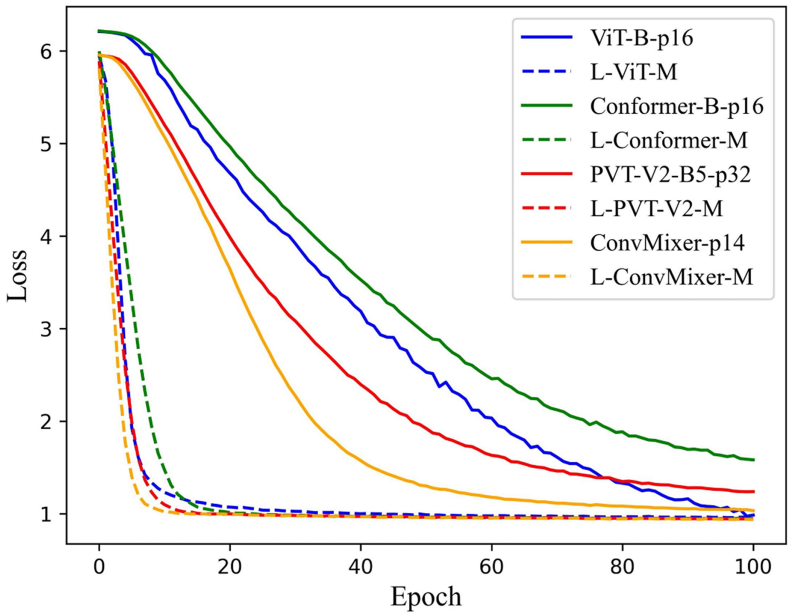

Figure 8 **Loss function on PolyU II dataset.** Full-size DOI: 10.7717/peerj-cs.3109/fig-8

Table 12 **Performance comparison of deep model.**

CompC	Flops (G)	MAdd (M)	Memory (M)
CCNet (*Yang et al., 2023a*)	0.257	0.514	5.89
CO3Net (*Yang et al., 2023b*)	0.11	0.22	3.07
EEPNet (*Jia et al., 2022*)	0.391	0.775	49.66
L-ViT (Proposed)	0.4	0.8	293.12
L-Conformer (Proposed)	26.73	53.31	818.68
L-PVT-V2 (Proposed)	1.44	2.85	315.40
L-ConvMixer (Proposed)	51.29	102.45	738.01

long as the model training is completed. In addition, PolyU II data set is a controlled environment database, so traditional methods usually have better results, while IIT Delhi, XINHUA, NTU-CP-V1 and BJTU are more complex databases, so deep learning methods typically achieve better performance. Compared with other depth palmprint methods, the determining conditions of computational complexity usually include Flops, MAdd and Memory. In order to be fair, the input of all depth models is scaled to 224 * 224. Table 12 presents the performance comparison of deep models.

As shown in Table 12, LViT has higher Flops, MAdd and memory size than CCNet, CO3Net and EEPNet, which is consistent with expectations. LViT divides the image into multiple patches for processing, which results in higher computational complexity. The self-attention mechanism needs to calculate the attention scores between all patches, and the embedding of each patch requires matrix multiplication and nonlinear transformations, which increases the computational burden. LViT contains a large number

of layers, which are used to capture complex image features, resulting in increased computational and memory consumption.

The complexity of LViT mainly depends on two aspects: the resolution of the input image and the sequence length of the image (the number of patches). Generally speaking, assuming that the resolution of the input image is $H \times W$, and the size of each patch is $P \times P$, then the image is divided into $(H \times W)/P^2$ patches. Assuming that the sequence length is N, LViT uses a multi-layer self-attention mechanism (self-attention), and the complexity is roughly $O(N^2 \times D)$, where D is the dimension of the vector representation of each patch. In each Transformer block, in addition to the self-attention, it also includes a fully connected multi-layer perceptron (MLP) layer. The complexity of the MLP layer is $O(N \times M^2)$, where M is the dimension of the hidden layer in the MLP layer. Therefore, the overall complexity of LViT can usually be expressed as $O((H \times W)/P^2 \times N^2 \times D + (H \times W)/P^2 \times N \times M^2)$.

Despite these higher computational costs, LViT has demonstrated superior performance in classification tasks, indicating that the benefits of its architectural design outweigh the associated computational overhead. Efforts to optimize LViTs' efficiency through techniques such as efficient attention mechanisms, model distillation, and pruning are ongoing research areas aimed at reducing their computational requirements while maintaining high performance. Recently, some lightweight ViTs (*Anasosalu Vasu et al., 2023*; *Mehta & Rastegari, 2022*; *Wang et al., 2024*) also provide the possibility of LViT extension, and the ViT-based methods will gradually improve performance to adapt to various devices. In addition, binary network and hash retry technology are new directions of consideration, which can map high-dimensional image data into low-dimensional binary coding space, reduce data storage and computational costs, and improve retrieval efficiency.

LViT finds the optimal model through various blocking strategies, which also have guiding role for non-Transformer-based neural networks. For example, it can use multi-scale CNN to perform tasks, take images of different scales as input and fusing the results of multiple branches for prediction. In addition, we can also combine the early stop mechanism in neural architecture search (NAS) to find the best partition, and customize a special LViT model for each database, which can greatly increase the computational complexity.

CONCLUSIONS

In this article, we explore depth palmprint recognition technology. Starting from the most important principal line features of palmprint, WLE data augmentation is proposed to obtain the principal line features of palmprint, resulting good recognition effect, with a maximum gain of 47.88%. At the same time, this article proposes the LViT paradigm for fusion output, which reduces training time and improves recognition accuracy. LViT provides new insights for direction-based methods in the field of palmprint recognition. In addition, this article simulates palmprint collection in the real-world environments, and carries out anti-noise experiments on the noise dataset to verify that LViT maintains high robustness and strong generalization ability in the harsh environment, especially with the

recognition rate on the PolyU II dataset reaching 99.53%, showing minimal impact. Although LViT accelerates model convergence, it also brings inevitable increases in memory pressure and computational cost. In the future, lightweight ViT methods will be explored and binary networks and hash retrieval technology will be introduced to compress the model to improve the retrieval efficiency.

ADDITIONAL INFORMATION AND DECLARATIONS

Funding

The work was supported by the Natural Science Foundation of the Anhui Xinhua University (No. 2023zr003), the Anhui Provincial Quality Engineering Project (No. 2023sx136, No. 2023xsxx356, No. 2020ylzy01) and the Key Research Project of Natural Science in Universities of Anhui Province (No. 2024AH050614, No. 2024AH050621, No. 2024AH050612). There was no additional external funding received for this study. The funders had no role in study design, data collection and analysis, decision to publish, or preparation of the manuscript.

Grant Disclosures

The following grant information was disclosed by the authors:
Natural Science Foundation of the Anhui Xinhua University: 2023zr003.
Anhui Provincial Quality Engineering Project: 2023sx136, 2023xsxx356, 2020ylzy01.
Key Research Project of Natural Science in Universities of Anhui Province: 2024AH050614, 2024AH050621, 2024AH050612.

Competing Interests

The authors declare that they have no competing interests.

Author Contributions

- Hongxia Wang conceived and designed the experiments, performed the experiments, analyzed the data, performed the computation work, prepared figures and/or tables, and approved the final draft.
- Teng Lv performed the computation work, authored or reviewed drafts of the article, and approved the final draft.

Data Availability

The following information was supplied regarding data availability:

The PolyU II Palmprint Database is available at:

- https://www4.comp.polyu.edu.hk/~csajaykr/palmprint3.htm
- Nebraska-Hewel. (2025). HewelXX/PolyUII: Palmprint PolyU II Dataset (v1.0.0). Zenodo. https://doi.org/10.5281/zenodo.16169889

The IIT Delhi Touchless Palmprint Database is available at: http://www4.comp.polyu.edu.hk/~csajaykr/IITD/Database_Palm.htm

The NTU Contactless Palmprints Database (NTU-CP-v1) is available at: https://github.com/matkowski-voy/Palmprint-Recognition-in-the-Wild

The BJTU_PalmV2 (BJTU-V2) dataset is available at GitHub: https://github.com/HewelXX/Dataset/tree/main/BJTU_V2

XINHUA Palmprint Database is available at GitHub and Zenodo:

- https://github.com/HewelXX/Dataset/tree/main/XINHUA

- Nebraska-Hewel. (2025). HewelXX/Dataset: Palmprint Dataset (v1.0.0) [Data set]. Zenodo. https://doi.org/10.5281/zenodo.15473268

Supplemental Information

Supplemental information for this article can be found online at http://dx.doi.org/10.7717/peerj-cs.3109#supplemental-information.

REFERENCES

Ali MMH, Yannawar P, Gaikwad AT. 2016. Study of edge detection methods based on palmprint lines. In: *International Conference on Electrical, Electronics, and Optimization Techniques, ICEEOT 2016* DOI 10.1109/ICEEOT.2016.7754902.

Anasosalu Vasu PK, Gabriel J, Zhu J, Tuzel O, Ranjan A. 2023. FastViT: a fast hybrid vision transformer using structural reparameterization. In: *Proceedings of the IEEE International Conference on Computer Vision*. Piscataway: IEEE DOI 10.1109/ICCV51070.2023.00532.

Biradar S. 2013. Personal identification using palmprint biometrics based on principal line approach. *International Journal of Advanced Research in Computer Engineering & Technology* **2**:2262–2267.

Bruno A, Carminetti P, Gentile V, La Cascia M, Mancino E. 2014. Palmprint principal lines extraction. In: *2014 IEEE Workshop on Biometric Measurements and Systems for Security and Medical Applications (BIOMS) Proceedings*. Piscataway: IEEE, 50–56 DOI 10.1109/BIOMS.2014.6951535.

Chai T, Prasad S, Wang S. 2019. Boosting palmprint identification with gender information using DeepNet. *Future Generation Computer Systems* **99(10)**:41–53 DOI 10.1016/j.future.2019.04.013.

Chen Z, Song D. 2023. Modeling landslide susceptibility based on convolutional neural network coupling with metaheuristic optimization algorithms. *International Journal of Digital Earth* **16(1)**:3384–3416 DOI 10.1080/17538947.2023.2249863.

Cubuk ED, Zoph B, Shlens J, Le QV. 2020. Randaugment: practical automated data augmentation with a reduced search space. In: *IEEE Computer Society Conference on Computer Vision and Pattern Recognition Workshops*. Piscataway: IEEE DOI 10.1109/CVPRW50498.2020.00359.

Davis LS, Rosenfeld A, Agrawala AK. 1976. On models for line detection. *IEEE Transactions on Systems, Man and Cybernetics* **SMC-6(2)**:127–133 DOI 10.1109/TSMC.1976.5409183.

Di HP, Shi JS, Xu GH. 2013. An associated extraction method of palmprint principal lines. In: *Proceedings—2013 7th International Conference on Image and Graphics, ICIG 2013*. Piscataway: IEEE DOI 10.1109/ICIG.2013.101.

Dosovitskiy A, Beyer L, Kolesnikov A, Weissenborn D, Zhai X, Unterthiner T, Dehghani M, Minderer M, Heigold G, Gelly S, Uszkoreit J, Houlsby N. 2021. An image is worth 16×16 words: transformers for image recognition at scale. In: *ICLR 2021—9th International Conference on Learning Representations*.

Fei L, Lu G, Jia W, Teng S, Zhang D. 2019. Feature extraction methods for palmprint recognition: a survey and evaluation. *IEEE Transactions on Systems, Man, and Cybernetics: Systems* **49(2)**:346–363 DOI 10.1109/TSMC.2018.2795609.

Huang DS, Jia W, Zhang D. 2008. Palmprint verification based on principal lines. *Pattern Recognition* **41(4)**:1316–1328 DOI 10.1016/j.patcog.2007.08.016.

Iula A, Nardiello D. 2016. A method for biometric recognition of ultrasound palmprint based on principal lines. *International Journal of Future Computer and Communication* **5(1)**:13–17 DOI 10.18178/ijfcc.2016.5.1.435.

Jain DK, Zhao X, González-Almagro G, Gan C, Kotecha K. 2023. Multimodal pedestrian detection using metaheuristics with deep convolutional neural network in crowded scenes. *Information Fusion* **95(6)**:401–414 DOI 10.1016/j.inffus.2023.02.014.

Jia W, Huang DS, Zhang D. 2008. Palmprint verification based on robust line orientation code. *Pattern Recognition* **41(5)**:1504–1513 DOI 10.1016/j.patcog.2007.10.011.

Jia W, Ren Q, Zhao Y, Li S, Min H, Chen Y. 2022. EEPNet: an efficient and effective convolutional neural network for palmprint recognition. *Pattern Recognition Letters* **159**:140–149 DOI 10.1016/j.patrec.2022.05.015.

Jia W, Zhou X. 2024. Improved high-resolution network for palmprint principal line extraction. In: Jabbar MA, Lorenz P, eds. *Third International Conference on Electronic Information Engineering and Data Processing (EIEDP 2024)*. Bellingham: SPIE, 150.

Jia W, Zhu YH, Liu LF, Huang DS. 2009. Fast palmprint retrieval using principal lines. In: *Conference Proceedings—IEEE International Conference on Systems, Man and Cybernetics*. Piscataway: IEEE DOI 10.1109/ICSMC.2009.5346694.

Kalluri HK, Prasad MVNK, Agarwal A. 2012. Palmprint identification based on wide principal lines. In: *ACM International Conference Proceeding Series*. New York: ACM DOI 10.1145/2345396.2345544.

Kumar A, Shekhar S. 2011. Personal identification using multibiometrics rank-level fusion. *IEEE Transactions on Systems, Man and Cybernetics Part C: Applications and Reviews* **41(5)**:743–752 DOI 10.1109/TSMCC.2010.2089516.

Li S, Fei L, Zhang B, Ning X, Wu L. 2024. Hand-based multimodal biometric fusion: a review. *Information Fusion* **109(12)**:102418 DOI 10.1016/j.inffus.2024.102418.

Li C, Liu F, Zhang Y. 2010. A principal palm-line extraction method for palmprint images based on diversity and contrast. In: *Proceedings—2010 3rd International Congress on Image and Signal Processing, CISP 2010*. Piscataway: IEEE DOI 10.1109/CISP.2010.5647934.

Li W, Zhang L, Zhang D, Yan J. 2009. Principal line based ICP alignment for palmprint verification. In: *Proceedings—International Conference on Image Processing, ICIP*. Piscataway: IEEE DOI 10.1109/ICIP.2009.5413459.

Liao F, Wu T, Gao F, Leng L. 2024. Translational calibration in region-of-interest localization for palmprint recognition. *The Visual Computer* **40(10)**:7293–7305 DOI 10.1007/s00371-024-03378-3.

Liu L, Zhang D. 2005. Palm-line detection. In: *Proceedings—International Conference on Image Processing, ICIP*. Piscataway: IEEE DOI 10.1109/ICIP.2005.1530380.

Liu L, Zhang D, You J. 2007. Detecting wide lines using isotropic nonlinear filtering. *IEEE Transactions on Image Processing* **16(6)**:1584–1595 DOI 10.1109/TIP.2007.894288.

Loshchilov I, Hutter F. 2018. Fixing weight decay regularization in Adam. *Available at https://arxiv.org/abs/1711.05101v1*.

Luo YT, Zhao LY, Zhang B, Jia W, Xue F, Lu JT, Zhu YH, Xu BQ. 2016. Local line directional pattern for palmprint recognition. *Pattern Recognition* **50(7)**:26–44 DOI 10.1016/j.patcog.2015.08.025.

Matkowski WM, Chai T, Kong AWK. 2020. Palmprint recognition in uncontrolled and uncooperative environment. *IEEE Transactions on Information Forensics and Security* **15**:1601–1615 DOI 10.1109/TIFS.2019.2945183.

Mehta S, Rastegari M. 2022. MobileViT: light-weight, general-purpose, and mobile-friendly vision transformer. In: *ICLR 2022—10th International Conference on Learning Representations*.

Minaee S, Abdolrashidi A, Su H, Bennamoun M, Zhang D. 2023. Biometrics recognition using deep learning: a survey. *Artificial Intelligence Review* **56(8)**:8647–8695 DOI 10.1007/s10462-022-10237-x.

Mousapour Mamoudan M, Ostadi A, Pourkhodabakhsh N, Fathollahi-Fard AM, Soleimani F. 2023. Hybrid neural network-based metaheuristics for prediction of financial markets: a case study on global gold market. *Journal of Computational Design and Engineering* **10(3)**:1110–1125 DOI 10.1093/jcde/qwad039.

Parulan DLM, Borcelis JNP, Linsangan NB. 2024. Palm lines recognition using dynamic image segmentation. In: *2024 IEEE International Conference on Automatic Control and Intelligent Systems (I2CACIS)*. Piscataway: IEEE, 238–243 DOI 10.1109/I2CACIS61270.2024.10649843.

Peng Z, Huang W, Gu S, Xie L, Wang Y, Jiao J, Ye Q. 2021. Conformer: local features coupling global representations for visual recognition. In: *Proceedings of the IEEE International Conference on Computer Vision*. Piscataway: IEEE DOI 10.1109/ICCV48922.2021.00042.

Putra IKGD, Witarsyah D, Saputra M, Jhonarendra P. 2021. Palmprint recognition based on edge detection features and convolutional neural network. *International Journal on Advanced Science, Engineering and Information Technology* **11(1)**:380–387 DOI 10.18517/ijaseit.11.1.11664.

Rotinwa-Akinbile MO, Aibinu AM, Salami MJE. 2011. Palmprint recognition using principal lines characterization. In: *Proceedings—1st International Conference on Informatics and Computational Intelligence, ICI 2011*. Piscataway: IEEE DOI 10.1109/ICI.2011.53.

Ruan S, Li Y, Qin H. 2024. LSFM: light style and feature matching for efficient cross-domain palmprint recognition. *IEEE Transactions on Information Forensics and Security* **19(1)**:9598–9612 DOI 10.1109/TIFS.2024.3476978.

Sathish R, Baskar D, Kumar DV. 2021. Palmprint biometric system using line based feature extraction methods. DOI 10.4108/eai.7-6-2021.2308682.

Shao H, Zhong D, Du X. 2019. Cross-domain palmprint recognition based on transfer convolutional autoencoder. In: *Proceedings—International Conference on Image Processing, ICIP*. Piscataway: IEEE DOI 10.1109/ICIP.2019.8803778.

Sun Z, Tan T, Wang Y, Li SZ. 2005. Ordinal palmprint represention for personal identification. In: *Proceedings—2005 IEEE Computer Society Conference on Computer Vision and Pattern Recognition, CVPR 2005*. Piscataway: IEEE DOI 10.1109/CVPR.2005.267.

Trockman A, Kolter JZ. 2022. Patches are all you need? ArXiv DOI 10.48550/arXiv.2201.09792.

Wang H, Cao X. 2025. Palmprint recognition using bifurcation line direction coding. *IEEE Access* **13**:70366–70377 DOI 10.1109/ACCESS.2025.3562648.

Wang A, Chen H, Lin Z, Han J, Ding G. 2024. Rep ViT: revisiting mobile CNN from ViT perspective. In: *2024 IEEE/CVF Conference on Computer Vision and Pattern Recognition (CVPR)*. Piscataway: IEEE, 15909–15920 DOI 10.1109/CVPR52733.2024.01506.

Wang H, Mariano VY. 2024. Fast local ordinal code for small sample palmprint recognition. *IEEE Access* **12(3)**:81867–81888 DOI 10.1109/ACCESS.2024.3408270.

Wang W, Xie E, Li X, Fan DP, Song K, Liang D, Lu T, Luo P, Shao L. 2021. Pyramid vision transformer: a versatile backbone for dense prediction without convolutions. In: *Proceedings of*

the IEEE International Conference on Computer Vision. Piscataway: IEEE DOI 10.1109/ICCV48922.2021.00061.

Wang W, Xie E, Li X, Fan DP, Song K, Liang D, Lu T, Luo P, Shao L. 2022. PVT v2: improved baselines with pyramid vision transformer. *Computational Visual Media* **8(3)**:415–424 DOI 10.1007/s41095-022-0274-8.

Wang Y, Zhao J, Sun G, Wang H, Chen X, Xu D. 2013. Palm lines extraction using PCNN and image data field. In: *2013 1st International Symposium on Future Information and Communication Technologies for Ubiquitous HealthCare, Ubi-HealthTech 2013* DOI 10.1109/Ubi-HealthTech.2013.6708065.

Wu X, Wang K, Zhang D. 2002. Line feature extraction and matching in palmprint. In: *Second International Conference on Image and Graphics* DOI 10.1117/12.477200.

Wu X, Zhang D. 2006. Palm line extraction and matching for personal authentication. *IEEE Transactions on Systems, Man, and Cybernetics Part A: Systems and Humans* **36(5)**:978–987 DOI 10.1109/TSMCA.2006.871797.

Wu X, Zhang D, Wang K, Huang B. 2004. Palmprint classification using principal lines. *Pattern Recognition* **37(10)**:1987–1998 DOI 10.1016/j.patcog.2004.02.015.

Xin G, Zhu M, Zhou Y, Jiang G, Cai Z, Pang A, Zhu Q. 2024. A self-attention CycleGAN for cross-domain semi-supervised contactless palmprint recognition. *International Journal of Image and Graphics* **24(02)**:279 DOI 10.1142/S0219467824500256.

Yang Z, Huangfu H, Leng L, Zhang B, Teoh ABJ, Zhang Y. 2023a. Comprehensive competition mechanism in palmprint recognition. *IEEE Transactions on Information Forensics and Security* **18**:5160–5170 DOI 10.1109/TIFS.2023.3306104.

Yang Z, Xia W, Qiao Y, Lu Z, Zhang B, Leng L, Zhang Y. 2023b. CO3Net: coordinate-aware contrastive competitive neural network for palmprint recognition. *IEEE Transactions on Instrumentation and Measurement* **72**:1–14 DOI 10.1109/TIM.2023.3276506.

Yuan W, Lin S, Tong H, Liu S. 2011. A detection method of palmprint principal lines based on local minimum gray value and line following. In: *2011 International Conference on Hand-Based Biometrics, ICHB, 2011—Proceedings*. Piscataway: IEEE DOI 10.1109/ICHB.2011.6094300.

Zhang D, Kong WK, You J, Wong M. 2003. Online palmprint identification. *IEEE Transactions on Pattern Analysis and Machine Intelligence* **25(9)**:1041–1050 DOI 10.1109/TPAMI.2003.1227981.

Zhao K, Shen L, Zhang Y, Zhou C, Wang T, Zhang R, Ding S, Jia W, Shen W. 2022. BézierPalm: a free lunch for palmprint recognition. In: *Lecture Notes in Computer Science (including subseries Lecture Notes in Artificial Intelligence and Lecture Notes in Bioinformatics)*. Cham: Springer.

Zivkovic M, Bacanin N, Antonijevic M, Nikolic B, Kvascev G, Marjanovic M, Savanovic N. 2022. Hybrid CNN and XGBoost model tuned by modified arithmetic optimization algorithm for COVID-19 early diagnostics from X-ray images. *Electronics* **11(22)**:3798 DOI 10.3390/electronics11223798.